Available online at www.sciencedirect.com
ScienceDirect
Journal of Sound and Vibration 319 (2009) 1252–1270
JOURNAL OF SOUND AND VIBRATION
www.elsevier.com/locate/jsvi

Unsteady loading on an airfoil of arbitrary thickness

Stewart A.L. Glegg[a,*], William Devenport[b,1]

[a]Department of Ocean Engineering, Florida Atlantic University, Boca Raton, FL 33431, USA
[b]Department of Aerospace and Ocean Engineering, Virginia Polytechnic and State University, Blacksburg, VA 26061, USA

Received 15 May 2007; received in revised form 29 May 2008; accepted 20 June 2008
Handling Editor: S. Bolton
Available online 15 August 2008

Abstract

The unsteady loading on an airfoil of arbitrary thickness is evaluated by using the generalized form of Blasius theorem and a conformal mapping that maps the airfoil surface onto a circle. For a blade vortex interaction the results show that the time history of the unsteady loading is determined by the passage of the vortex relative to the leading edge singularity in the circle plane. The singularity lies inside the circle and moves to a smaller radius as the thickness is increased, causing the unsteady loading pulse to be smoothed. The effect of angle of attack is to move the stagnation point relative to the leading edge singularity and this significantly increases the unsteady lift if the vortex passes on the suction side of the airfoil. These characteristics are different for a step upwash gust, which is considered as a simplified model of a large scale turbulent gust. It is shown that the time history of the magnitude of the unsteady loading is almost completely unaltered by angle of attack for the step gust, but it's direction of action rotates forward by an angle equal to the angle of attack, extending an earlier result by Howe for a flat plate in a turbulent flow to airfoils of arbitrary thickness. However spectral analysis of the gust shows that the high frequency blade response is reduced as the thickness of the airfoil is increased.

1. Introduction

The unsteady loading on an airfoil caused by an incident gust is important in many applications and has received significant attention in the literature. The problem of a two-dimensional flat plate airfoil in a uniform flow encountering a harmonic upwash gust was addressed by Sears [1]. Amiet and Sears [2] extended the solution to three dimensions for airfoils of large chord. Goldstein and Atassi [3] provided an asymptotic solution for a two-dimensional potential flow over an airfoil of finite thickness, camber and angle of attack based on the assumptions of thin airfoil theory. Atassi [4] showed how this solution could be split into three independent terms that separated the effects of thickness, camber and angle of attack. Howe [5] gave a formula for the unsteady loading on a body of arbitrary shape based on a volume integral of a Greens function and the Lamb vector of the unsteady flow. He showed [6] that, for a flat plate in a turbulent flow the unsteady lift was rotated forward as the angle of attack was increased. In Howe [7] it was shown that, for a stationary airfoil,

*Corresponding author. Tel.: +1 561 297 2633.
E-mail addresses: glegg@oe.fau.edu (S.A.L. Glegg), devenport@vt.edu (W. Devenport).
[1]Tel.: +1 540 240 4456.

0022-460X/$ - see front matter © 2008 Elsevier Ltd. All rights reserved.
doi:10.1016/j.jsv.2008.06.053

the unsteady loading could be obtained using a surface integral over the body in which the integrand is a Greens function multiplied by the velocity induced by the vorticity in the flow. It was also shown [7–9] that the unsteady loading is strongly affected by the application of the Kutta condition at the trailing edge of the airfoil. If the Kutta condition is not applied the time history of the unsteady loading exhibits a pulse as the gust passes the trailing edge. If the Kutta condition is applied, and disturbances in the wake are convected at the speed of the mean flow, then the pulse generated as the gust passes the trailing edge is completely cancelled. By ignoring the trailing edge Howe [7] showed that the unsteady blade response approximated Sears function for non-dimensional frequencies $\sigma = \omega b/U > 1$, where b is the semichord, U is the free stream velocity and ω is the angular frequency of the unsteady load. Gershfeld [10] considered a turbulent gust incident on a flat plate of finite thickness and showed that the radiated sound was reduced at high frequencies as the thickness was increased. Similar results were obtained by Martinez and Rudzynsky [11] and Grace [12] for blade vortex interactions. Numerical methods such as the unsteady panel method described by Grace [12] or computational methods based on the Navier Stokes equations, as described by Lockard and Morris [13], have given the solution for the unsteady loading on airfoils of arbitrary shape.

In this paper we will show that the unsteady loading on a two-dimensional airfoil in an incompressible potential flow can be obtained using the generalized form of Blasius's theorem. The contribution of this approach is that it shows directly the physical impact of both thickness and angle of attack on the unsteady loading, without being limited by the assumptions of thin airfoil theory. It is shown that the characteristics of the response to a blade vortex interaction are quite different from the response to a step upwash gust. The blade vortex interaction is very sensitive to the effect of angle of attack, but this is not the case for a step gust. It is found that, for the step gust, the time history of the magnitude of the unsteady lift is almost unaltered by angle of attack, but its direction of action is rotated forward as the angle of attack is increased. This agrees with and extends Howe's [6] result for a flat plate to airfoils of arbitrary thickness. However spectral analysis of the gust shows that the high frequency blade response is reduced as the thickness of the airfoil is increased.

2. Unsteady loading on an airfoil

2.1. The unsteady flow

The unsteady loading will be calculated for a gust incident on an airfoil at rest in a uniform mean flow. The fluid will be assumed to be inviscid, incompressible and two dimensional so the unsteady loading can be obtained from potential flow theory. The complex potential of the flow is defined as $W(Z)$, (where $Z = X + \mathrm{i}Y$ and (X, Y) represents a point in the physical plane), and can be obtained by mapping the airfoil surface onto a circle in the complex z-plane using the transformation

$$Z = (z-\lambda) + (a-\lambda)^2/(z-\lambda) \quad (z-\lambda) = Z/2 + \sqrt{Z^2/4 - (a-\lambda)^2}, \tag{1}$$

where a is the radius of the circle and λ is a lengthscale to be defined below. For a Joukowski airfoil at an angle of attack α, in a flow with uniform speed U, the complex potential is given (see for example Ref. [14]) as

$$W_0(Z) = w_0(z) = Uz\,\mathrm{e}^{-\mathrm{i}\alpha} + \frac{Ua^2\,\mathrm{e}^{\mathrm{i}\alpha}}{z} - \frac{\mathrm{i}\Gamma}{2\pi}\ln(z), \tag{2}$$

where the airfoil chord is $4a^2/(a+\lambda)$ and its thickness to chord ratio is given by $3\sqrt{3}\lambda(a+\lambda)/(4a^2)$. For thin airfoils $\lambda \ll 1$ the chord is approximately $4a$ and the blade thickness to chord ratio is 5.2λ. The surface of the airfoil is defined by the circle of radius a in the z-plane centered at $z = 0$ and the trailing edge of the airfoil lies at $z = a$. To satisfy the Kutta condition the mean circulation about the airfoil is given by $\Gamma = -4\pi Ua\sin\alpha$.

To calculate the unsteady loading on the airfoil we will consider the incident gust to be a point vortex of strength γ_0 that is convected with the mean flow. Howe [8] has shown that the response of the airfoil to an incident vortex is equivalent to the harmonic gust problem considered by Sears [1] and Goldstein and Atassi [3]. These results assume Rapid Distortion Theory (RDT) [15–17], which requires that the vortex is convected by the mean flow without being displaced by its image vortex inside the airfoil. This assumption cannot be applied for a vortex which is convected along the stagnation streamline upstream of the leading edge because

the vortex will come rest at the stagnation point. However this is not realizable for a vortex with non-zero strength because the image vorticity will displace the vortex from the stagnation point and it will then be convected by the adjacent flow. The issue of gust distortion next to the stagnation point can lead to numerical errors for harmonic gust descriptions [18] but these are avoided by describing the incident gust as a point vortex providing it is not located precisely on the stagnation streamline.

In this analysis we will assume Rapid Distortion Theory which requires that the vortex is convected by the mean flow along a streamline without change in strength and we will avoid the issue of gust distortion at the stagnation point by not placing a vortex on the stagnation streamline in numerical calculations. The vortex position is then relatively easy to calculate and will by specified as $z_0(t)$ in the circle plane. The velocity potential induced by the vortex and its image inside the circle is then

$$w_v(z,t) = -\frac{\mathrm{i}\gamma_0}{2\pi}\ln(z-z_0) + \frac{\mathrm{i}\gamma_0}{2\pi}\ln(z_I - z) - \frac{\mathrm{i}\gamma_0}{2\pi}\ln(z/z_0^*), \tag{3}$$

where $z_I = a^2/z_0^*$ is the location of the image vortex. The potential specified in (3) satisfies the non-penetration boundary condition on the airfoil surface but does not satisfy the Kutta condition. This can be achieved by introducing a vorticity distribution in the wake downstream of the trailing edge which ensures that the unsteady velocity at the trailing edge is finite. If the potential induced by the wake is $w_w(z,t)$ then the unsteady Kutta condition requires that $w_v'(a,t) + w_w'(a,t) = 0$, where the prime represents a derivative with respect to the complex variable z. The wake will be assumed to lie on the x-axis in the circle plane so the velocity potential induced by the wake is

$$w_w(z,t) = \frac{-\mathrm{i}}{2\pi}\int_{-\infty}^{t} \mu(\tau)\{\ln(z - x_w(t,\tau)) - \ln(x_I(t,\tau) - z)\}\mathrm{d}\tau, \tag{4}$$

where $\mu(\tau)$ is the rate of change of vorticity at the trailing edge at time τ, $x_w(t,\tau)$ is the location of the vorticity at time t generated at the trailing edge at time τ and $x_I = a^2/x_w$. Note that $x_w(t,\tau) > x_w(\tau,\tau) = a+\varepsilon$ when $\tau < t$ and the small parameter $\varepsilon > 0$ ensures that the wake is initiated downstream of the trailing edge. To satisfy the Kutta condition we require that $w_v'(a,t) + w_w'(a,t) = 0$ and using Eq. (4) we obtain

$$w_v'(a,t) = \frac{\mathrm{i}}{2\pi}\int_{-\infty}^{t}\mu(\tau)\left(\frac{1}{(a-x_w)} - \frac{1}{(a-x_I)}\right)\mathrm{d}\tau = \frac{\mathrm{i}}{2\pi}\int_{-\infty}^{t}\mu(\tau)\left(\frac{x_w + a}{a(a-x_w)}\right)\mathrm{d}\tau. \tag{5}$$

Using Eqs. (3) and (5) we obtain an integral equation for the vorticity in the wake as

$$\int_{-\infty}^{t}\mu(\tau)\left(\frac{x_w + a}{x_w - a}\right)\mathrm{d}\tau = -\gamma_0\left(\frac{a}{(z_0 - a)} + \frac{a}{(z_0^* - a)}\right). \tag{6}$$

This integral can be solved by standard methods using Fourier transforms and will be discussed in more detail below. However it is worth noting here that $\mu(\tau)$ is real valued.

2.2. The unsteady loading

The unsteady loading on the airfoil can be calculated from the generalized form of Blasius theorem

$$F_X + \mathrm{i}F_Y = \left(\frac{\mathrm{i}\rho}{2}\oint_C\left(\frac{\mathrm{d}W}{\mathrm{d}Z}\right)^2\mathrm{d}Z\right)^* - \mathrm{i}\rho\frac{\mathrm{d}}{\mathrm{d}t}\oint_C W(Z)\mathrm{d}Z, \tag{7}$$

where the contour integral is carried out over the surface of the airfoil. The first integral represents the contribution from the circulation and will be represented by $(F_X + \mathrm{i}F_Y)_c$. In steady flow the integral is evaluated [14] by expanding the contour onto a circle with a large radius and then using a Laurent expansion to represents the integrand. This leads to the conclusion that the load due to circulation is given by $-\mathrm{i}\rho\Gamma U\exp(\mathrm{i}\alpha)$. However in unsteady flow the expansion of the contour to a large radius must take into account the vorticity in the wake and the presence of the vortex at Z_0. The same contour at a large radius can be used but the result must be modified by adding the contributions from the vortex and the wake. Since the wake does not support a discontinuity in pressure the contour C used in both integrals in Eq. (7) can be

extended to enclose the wake without changing the value of F_X+iF_Y. We can draw this extension from the suction side of the trailing edge, along the upper surface of the wake to a circular contour of large radius, and then along the lower side of the wake to the lower surface of the trailing edge. The contour must be indented to bypass the singularity at the vortex located at Z_0. The circulation load can then be defined by the combination of two contour integrals as

$$(F_X + \mathrm{i}F_Y)_c = \left(\frac{\mathrm{i}\rho}{2} \left\{ \oint_{C_1} - \oint_{C_2} \right\} \left(\frac{\mathrm{d}W}{\mathrm{d}Z} \right)^2 \mathrm{d}Z \right)^* . \tag{8}$$

The path C_1 represents a circular contour of a large radius (but not so large that the starting vortex is inside the contour) centered at the origin, and the C_1 contour integral can be evaluated using a Laurent series as before. The result will be given by the total circulation, including the contributions from the vortex and its images inside the surface, which sum to γ_0 and the wake vorticity and its image, which sum to zero. The net contribution to the circulation load will be $-\mathrm{i}\rho(\Gamma+\gamma_0)U\exp(\mathrm{i}\alpha)$. The contour C_2 represents a contour around the vortex at Z_0 and can be collapsed onto a small circle centered on the vortex location where we can represent the integrand as

$$\left(\frac{\mathrm{d}W}{\mathrm{d}Z} \right)^2 = \left(\frac{\mathrm{d}W_e(Z_0)}{\mathrm{d}Z} - \frac{\mathrm{i}\gamma_0}{2\pi(Z-Z_0)} \right)^2, \tag{9}$$

where $W_e(Z_0)$ represents the complex potential at Z_0 from all sources but the vortex itself. Using Rapid Distortion Theory implies that $\mathrm{d}W_e(Z_0)/\mathrm{d}Z$ is well approximated by the steady flow at Z_0 and so the integral over C_2 yields a contribution to the circulation load of $\mathrm{i}\rho\gamma_0 V(Z_0)$. The net circulation load is then given by

$$(F_X + \mathrm{i}F_Y)_c = -\mathrm{i}\rho\Gamma U\,\mathrm{e}^{\mathrm{i}\alpha} + \mathrm{i}\rho\gamma_0(V(Z_0) - U\,\mathrm{e}^{\mathrm{i}\alpha}). \tag{10}$$

The first term represents the steady load and the second gives the contribution to the unsteady load from the vortex attraction to the surface.

The second integral in Eq. (7) represents the added mass which will be identified by $(F_X$+i$F_Y)_m$. The integrand can be transformed to the z-plane and the contour carried out over the circle representing the surface of the airfoil and the extension enclosing the wake, giving

$$(F_X + \mathrm{i}F_Y)_m = -\mathrm{i}\rho \oint_C \frac{\partial w(z,t)}{\partial t} \frac{\mathrm{d}Z}{\mathrm{d}z} \mathrm{d}z. \tag{11}$$

First we will consider the case when there is no wake, and the Kutta condition is not satisfied, so the only contribution to this integral is from the potential induced by the vortex (Eq. (3)), which gives

$$\frac{\rho\gamma_0}{2\pi} \oint_C \left(1 - \frac{(a-\lambda)^2}{(z-\lambda)^2} \right) \left(\frac{1}{(z-z_0)} \frac{\mathrm{d}z_0}{\mathrm{d}t} - \frac{1}{(z-z_I)} \frac{\mathrm{d}z_I}{\mathrm{d}t} + \left(\frac{1}{z_0} \frac{\mathrm{d}z_0}{\mathrm{d}t} \right)^* \right) \mathrm{d}z. \tag{12}$$

Using the residue theorem to evaluate the integral and including the contributions from the second-order pole at $z=\lambda$ and the simple pole at $z=z_I$ gives the unsteady load due to the motion of the vortex as

$$(F_x + \mathrm{i}F_y)_v = \mathrm{i}\rho\gamma_0 \left\{ \frac{(a-\lambda)^2}{(z_0-\lambda)^2} \left(\frac{\mathrm{d}z_0}{\mathrm{d}t} \right) - \left(\frac{\mathrm{d}z_I}{\mathrm{d}t} \right) \right\} = \mathrm{i}\rho\gamma_o \left\{ \frac{(a-\lambda)^2}{(z_0-\lambda)^2} \left(\frac{\mathrm{d}z_0}{\mathrm{d}t} \right) + \left(\frac{a^2}{z_0^2} \frac{\mathrm{d}z_0}{\mathrm{d}t} \right)^* \right\}. \tag{13}$$

The time history of the unsteady loading described by Eq. (13) is clearly determined by the rate of vortex convection which can be specified using $V(Z_0)$ as

$$\frac{\mathrm{d}z_0}{\mathrm{d}t} = \frac{\mathrm{d}z_0}{\mathrm{d}Z_0} \frac{\mathrm{d}Z_0}{\mathrm{d}t} = \frac{V(Z_0)}{1 - (a-\lambda)^2/(z_0-\lambda)^2}. \tag{14}$$

This has two peaks which occur when the vortex is at it's closest point to the leading or trailing edge singularities located at $z_0 = 2\lambda - a$ and $z_0 = a$. The time history of the unsteady load given by Eq. (13) will therefore have a leading and trailing edge pulse, which can be conveniently identified by expanding the first

term in Eq. (13) using partial fractions to give

$$\left(\frac{a-\lambda}{z_0-\lambda}\right)^2\frac{\mathrm{d}z_0}{\mathrm{d}t}=\frac{1}{2}\left(\frac{-(a-\lambda)V(Z_0)}{z_0+a-2\lambda}+\frac{(a-\lambda)V(Z_0)}{z_0-a}\right). \tag{15}$$

The first term represents the leading edge pulse while the second term represents the trailing edge pulse. The magnitude of these pulses will be discussed in more detail in Section 3.

To calculate the unsteady loading we must also include the added mass induced by the wake, which can be obtained from Eq. (11) using

$$(F_x+\mathrm{i}F_y)_w=-\mathrm{i}\rho\oint_C\left(1-\frac{(a-\lambda)^2}{(z-\lambda)^2}\right)\frac{\partial w_w}{\partial t}\mathrm{d}z, \tag{16}$$

where

$$\frac{\partial w_w}{\partial t}=\frac{\mathrm{i}}{2\pi}\int_{-\infty}^{t}\mu(\tau)\left\{\frac{1}{(z-x_w)}\frac{\partial x_w}{\partial t}-\frac{1}{(z-x_I)}\frac{\partial x_I}{\partial t}\right\}\mathrm{d}\tau+\frac{\mu(t)}{2}. \tag{17}$$

Applying the residue theorem to Eq. (16) over the contour which encloses both the airfoil surface and the wake gives a solution which only depends on the simple poles at $z=x_w$ and $z=x_I$. The unsteady load from the wake is then

$$(F_x+\mathrm{i}F_y)_w=\mathrm{i}\rho\int_{-\infty}^{t}\mu(\tau)\left\{1+\frac{a^2}{x_w^2}\right\}\frac{\partial x_w}{\partial t}\mathrm{d}\tau. \tag{18}$$

The integral in Eq. (18) clearly depends on the rate at which vorticity is convected in the wake. There has been much debate (see Ref. [9]) about the choice of convection speed and so we will proceed by allowing this to be a variable for the time being. In the Z-plane the wake convection velocity will be assumed to be $V(X_w)$ and so the convection velocity in the z-plane is

$$\frac{\mathrm{d}x_w}{\mathrm{d}t}=\frac{\mathrm{d}x_w}{\mathrm{d}X_w}\frac{\mathrm{d}X_w}{\mathrm{d}t}=\frac{V(X_w)}{1-(a-\lambda)^2/(x_w-\lambda)^2}, \tag{19}$$

and it follows that

$$(F_x+\mathrm{i}F_y)_w=\mathrm{i}\rho\int_{-\infty}^{t}\mu(\tau)\left(\left\{1+\frac{a^2}{x_w^2}\right\}\frac{(x_w-\lambda)^2V(X_w)}{(x_w-\lambda)^2-(a-\lambda)^2}\right)\mathrm{d}\tau. \tag{20}$$

The unsteady loading is then given by the sum of Eqs. (10), (13) and (20) which may be combined as

$$\begin{aligned}(F_x+\mathrm{i}F_y)_u=\mathrm{i}\rho\gamma_0\left\{\frac{(a-\lambda)^2}{(z_0-\lambda)^2}\left(\frac{\mathrm{d}z_0}{\mathrm{d}t}\right)+\left(\frac{a^2}{z_o^2}\frac{\mathrm{d}z_0}{\mathrm{d}t}\right)^*+V(Z_0)-U\,\mathrm{e}^{\mathrm{i}\alpha}\right\}\\+\mathrm{i}\rho\int_{-\infty}^{t}\mu(\tau)V(X_w)\left(\left\{1+\frac{a^2}{x_w^2}\right\}\frac{(x_w-\lambda)^2}{(x_w-\lambda)^2-(a-\lambda)^2}\right)\mathrm{d}\tau.\end{aligned} \tag{21}$$

The first term in Eq. (21) is easily calculated from the location and velocity of the vortex. The second term however depends on the time history of the wake vorticity and requires the evaluation of a convolution integral. It will be shown in Appendix A how this can be carried out using Fast Fourier Transforms.

Eq. (21) simplifies considerably for a flat plate at zero angle of attack for which $V(Z_0)=V(X_w)=U$ and $\alpha=\lambda=0$, so using Eq. (14) gives

$$(F_x+\mathrm{i}F_y)_u=2\mathrm{i}\rho\gamma_0U\,\mathrm{Re}\left(\frac{a^2}{z_0^2-a^2}\right)+\mathrm{i}\rho U\int_{-\infty}^{t}\mu(\tau)\left(\frac{x_w^2+a^2}{x_w^2-a^2}\right)\mathrm{d}\tau. \tag{22}$$

Expanding both terms using partial fractions gives

$$(F_x+\mathrm{i}F_y)_u=\mathrm{i}\rho\gamma_0U\,\mathrm{Re}\left(\frac{a}{z_0-a}-\frac{a}{z_0+a}\right)+\frac{\mathrm{i}\rho U}{2}\int_{-\infty}^{t}\mu(\tau)\left(\frac{x_w+a}{x_w-a}+\frac{x_w-a}{x_w+a}\right)\mathrm{d}\tau. \tag{23}$$

This shows that the vortex induces a pulse at $z_0 = -a$ and $z_0 = a$ but, by using Eq. (6), we see that the term dependent on $(z_0 - a)^{-1}$ exactly cancels the singularity of the convolution integral that occurs when $x_w = a$. Combining Eqs. (6) and (23) gives

$$(F_x + \mathrm{i}F_y) = -\mathrm{i}\rho\gamma_0 aU\,\mathrm{Re}\left\{\frac{1}{z_0 + a}\right\} + \frac{\mathrm{i}\rho U}{2}\int_{-\infty}^{t} \mu(\tau)\left(\frac{x_w - a}{x_w + a}\right)\mathrm{d}\tau. \tag{24}$$

The first term represents the leading edge pulse and the second the contribution from the wake. It will be shown in Appendix A that Eq. (24) reduces to the result that would have been obtained if the analysis had been carried out in the frequency domain using Sears function.

3. Discussion

3.1. Results for a flat plate

To verify the results given above we will first consider the case of a flat plate at zero angle of attack in a uniform flow for which the unsteady lift can be calculated using Sears function. Using Eq. (24) the unsteady loading can be split into two parts: the first is the leading edge pulse given by the first term in Eq. (24) and the second is the wake pulse given by the second term in Eq. (24). The leading edge pulse is relatively simple to evaluate from the potential mean flow, but the wake pulse requires the evaluation of a convolution integral which is more involved. It is shown in Appendix A how this can be solved using Fourier Transforms and an analytical solution is derived which reduces to the same result as would have been obtained by utilizing Sears function. The relative magnitude of the leading edge and wake pulses is illustrated in Fig. 1, which shows the unsteady lift $L(t) = F_y(t)$ for a vortex passing a distance $4a/10$ above a flat plate. The leading edge pulse clearly dominates and the wake pulse is only important as the vortex passes the mid chord point at time $Ut/a = 0$. The vortex passes the trailing edge at time $Ut/a = 2$ and both the leading edge and wake pulses show a sharp change in slope at this point. However the net effect is negligible as shown by the sum of the two pulses. The overall signature is dominated by the leading edge interaction, and the sharpness of the pulse depends on the distance of the vortex from the airfoil.

The spectra of the time histories $\tilde{L}(\omega)$ shown in Fig. 1 have been normalized by the upwash spectrum of the gust $\tilde{v}(\omega)$ (see Eq. (A.5)) and compared to Sears function in Fig. 2 as a function of the non-dimensional frequency $\sigma = 2\omega a/U$. The plots show the non-dimensional lift response function $S_L(\omega) = |\tilde{L}(\omega)/4\pi\rho aU\tilde{v}(\omega)|$. At non-dimensional frequencies $\sigma > 10$ the spectrum of the leading edge pulse is identical to Sears function, but at lower frequencies it exhibits an oscillatory behavior and asymptotes to 0.5 for $\sigma \ll 1$. The magnitude of the

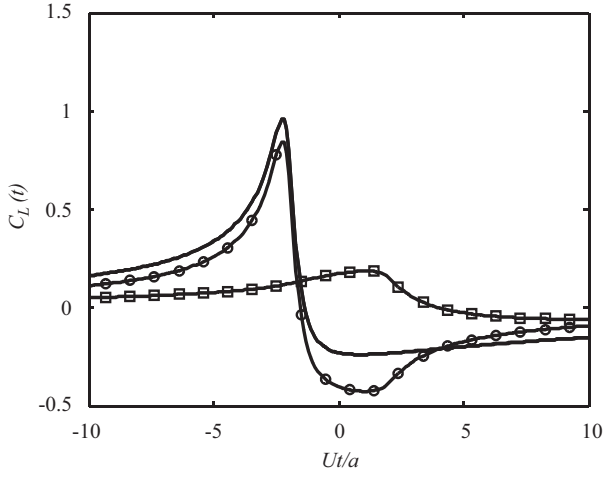

Fig. 1. The unsteady lift coefficient $C_L(t) = L(t)/\rho U\gamma_0$ for a vortex passing at a distance $4a/10$ above a flat plate: (– ○ –) leading edge pulse, (– □ –) pulse induced by the wake, (—) sum of the two pulses.

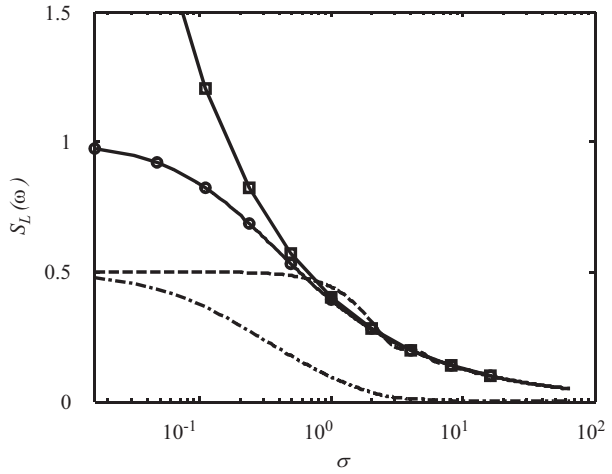

Fig. 2. Lift response function magnitude $S_L(\omega) = |\tilde{L}(\omega)/4\pi\rho a U\tilde{v}(\omega)|$ as a function of reduced frequency σ for a flat plate showing the contribution of the wake (– · –) and the leading edge (dashed line – –). The total unsteady lift (the Sears function) is presented both as the theoretical calculation (○) and as the sum of the leading edge and wake response (solid line). Also shown is the high-frequency approximation for Sears function (– □ –).

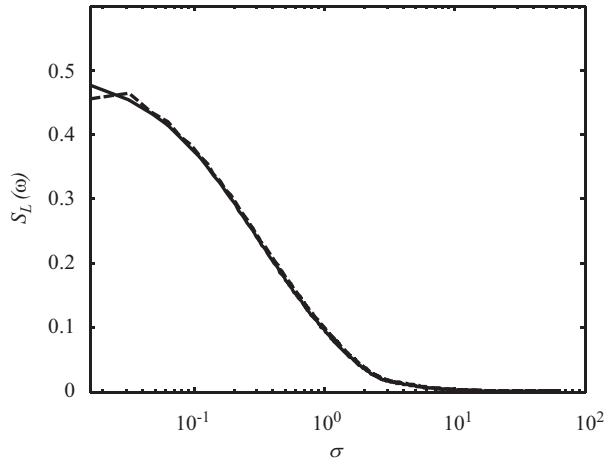

Fig. 3. Comparison between the lift response function $S_L(\omega) = |\tilde{L}(\omega)/4\pi\rho a U\tilde{v}(\omega)|$ induced by the wake of a flat plate calculated numerically (dashed line) and using the theoretical formulation (solid line) given in Appendix A. Note that errors are only significant at the lowest reduced frequencies. Number of points used in the transform is 8196 and the reduced frequency resolution is 0.0157.

contribution from the wake is also shown and this is clearly only important at low frequencies ($\sigma < 3$) The sum of the leading edge contribution and the wake contribution exactly matches the Sears function as shown. At low frequencies the leading edge and wake contributions are in phase and add to give a level which asymptotes to one. At non-dimensional frequencies $\sigma \sim 1$ the two terms are out of phase and the leading edge contribution is reduced by the wake contribution. It is also interesting to consider the high frequency approximation to the Sears function whose magnitude is given by $1/\sqrt{2\pi\sigma}$. This is a good approximation at non-dimensional frequencies $\sigma > 1$ but tends to infinity at low frequencies. In the frequency range $1 < \sigma < 10$ it is a better approximation than the leading edge response in isolation.

The evaluation of the convolution integral in Eq. (24) can also be carried out numerically using Fast Fourier Transforms, as shown in Appendix A. While this is not necessary for the flat plate, it will be required for an airfoil of finite thickness or at an angle of attack and so the accuracy of the numerical method needs to be established. Fig. 3 shows a comparison of the wake pulse calculated numerically and theoretically as a

function of frequency. It is seen that, apart from the lowest frequency bin, the error in the numerical method is very small and should give accurate results when applied to different configurations.

3.2. The effect of thickness and angle of attack

To demonstrate the effects of thickness and angle of attack on the unsteady loading Fig. 4 shows a calculation (using the approach described in Appendix A) for a vortex passing an airfoil with a thickness to chord ratio of 0.15, at three different angles of attack. The results are presented as lift and drag components where the lift is given as the unsteady loading normal to the direction of the flow, $L = \mathrm{imag}((F_X+\mathrm{i}F_Y)\exp(-\mathrm{i}\alpha))$ and the drag is in the direction of the flow and given by $D = \mathrm{real}((F_X+\mathrm{i}F_Y)\exp(-\mathrm{i}\alpha))$. The vortex is initiated at a point on a streamline which, at upstream infinity, would have been a distance equal to 10% of the chord above the stagnation streamline. The initiation point of the vortex should therefore be independent of the angle attack and thickness of the airfoil. Fig. 4 shows that the unsteady lift can be represented by a pulse which peaks as the vortex passes the leading edge, but, as in the case of the flat plate, there is no apparent trailing edge pulse. The amplitude of the leading edge pulse increases with angle of attack. In contrast the unsteady drag exhibits a leading edge pulse which is negative causing leading edge suction which increases with angle of attack. When the vortex has passed the leading edge the drag is positive and decays slowly to zero as the vortex progresses.

3.3. Response to a step function upwash gust

An alternative gust type is a step upwash gust which can be represented by a sheet of vorticity normal to the direction of the incident flow at upstream infinity. In a uniform mean flow, and assuming Rapid Distortion Theory, the gust convects without modifying itself and represents a step change in upwash velocity. The step gust, while unrealizable in practice, is a reasonable model for a large lengthscale turbulent gust, and the unsteady loading caused by a step gust will be indicative of the loading from the low wavenumber components of the turbulence spectrum. To model a step gust the vortex sheet is specified by the superposition of elemental vortices of strength $\gamma_0 = \Delta v \Delta h$ separated by the distance Δh where Δv is the magnitude of the velocity jump across the step gust. To avoid numerical errors we need to ensure that a vortex is not placed on the stagnation streamline (see Section 3.5 for numerical details).

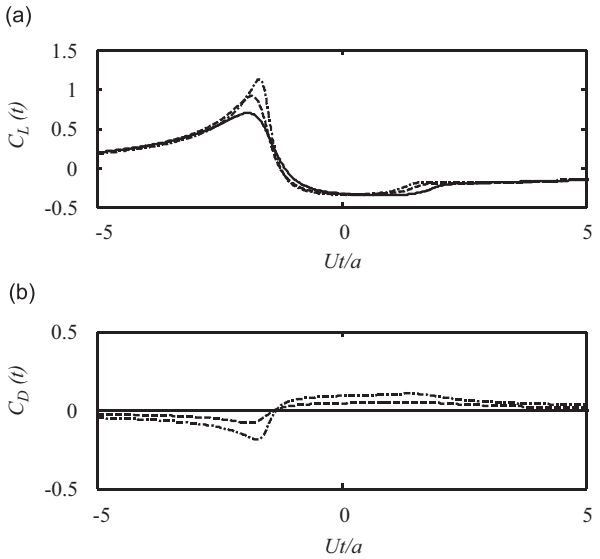

Fig. 4. (a) The unsteady lift coefficient $C_L(t) = L(t)/\rho U\gamma_0$ and (b) unsteady drag coefficient $C_D(t) = D(t)/\rho U\gamma_0$ for a vortex initiated at 10% of the chord above the stagnation streamline for airfoils at different angles of attack. Airfoil thickness to chord ratio is 0.15. Angle of attack: — 0°, – – 5°, – · – 10°.

The unsteady loading from a step gust can be calculated using the approach described above by summing the contributions from each elemental vortex and the results are presented in Fig. 5. In this case we expect (from Ref. [6]) that the effect of angle of attack on the unsteady loading will be to rotate the loading vector forward by an angle equal to the angle of attack. To illustrate this effect the results presented in Fig. 5 are for the forces relative to the direction of the loading suggested by Howe, which is rotated forward by 2α from the direction of the chord. This gives the forces $F_L = \mathrm{imag}((F_X+\mathrm{i}F_Y)\exp(-2\mathrm{i}\alpha))$ and $F_D = \mathrm{real}((F_X+\mathrm{i}F_Y)\exp(-2\mathrm{i}\alpha))$. If Howe's theory for a flat plate applies to an airfoil of finite thickness then the pulses shown in Fig. 5 should be independent of angle of attack, which is clearly the case for F_L. The force F_D shows a small increase with angle of attack but this is smoothly varying and relatively insignificant.

An explanation of the effects which are taking place as the airfoil thickness and angle of attack are changed is given by Fig. 6 which shows the flow about the airfoil in the circle plane. For a step gust a vortex will be convected along each of the streamlines shown in the figure and the amplitude of the leading edge pulse will

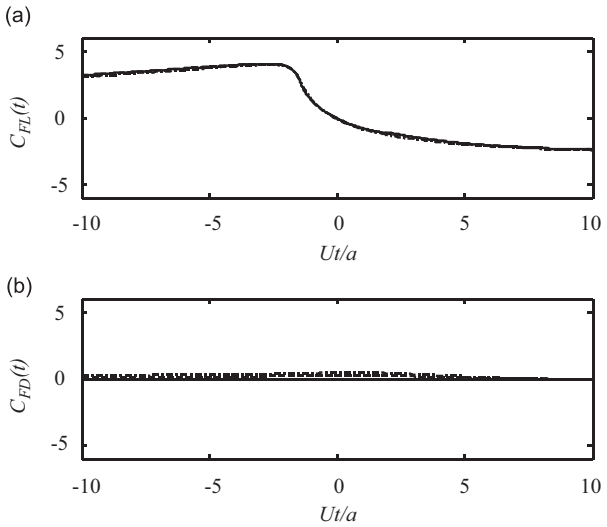

Fig. 5. The unsteady loading coefficients $C_{\mathrm{FL}}(t) = F_L(t)/\rho U\Delta va$ and $C_{\mathrm{FD}}(t) = F_D(t)/\rho U\Delta va$ for a step function incident on an airfoil at angles of attack of 0 (solid line), 4 (dashed line) and 8° (dashed dot line). Airfoil thickness to chord ratio is 0.15. The direction of the force component F_L (shown in (a)) is rotated forward from the lift force direction by an angle equal to the angle of attack, and the force F_D is normal to F_L.

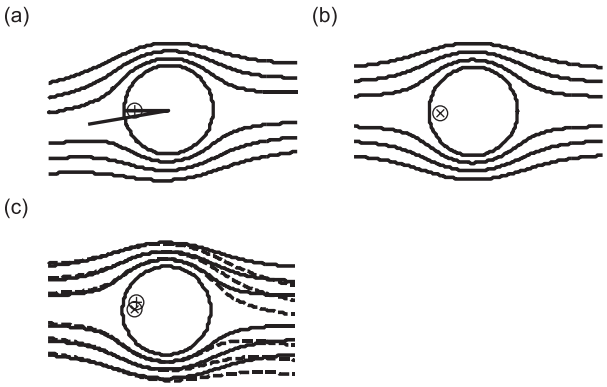

Fig. 6. Vortex trajectories in the circle plane showing that they are almost identical in the leading edge region for all angles of attack if the leading edge stagnation points are aligned: (a) vortex trajectories at 5° angle of attack, (b) vortex trajectories at 0° angle of attack, (c) overlay of (b) onto (a) rotated clockwise by twice the angle of attack. (×) location of singular pint for zero angle of attack, (+) location of singular pint for 5° angle of attack.

depend on the distance of the vortices from the leading edge singular point which is located at $z = -a+2\lambda$ and shown in the figure by the small circle. The effect of increasing the airfoil thickness is to move the singular point to a smaller radius, which will cause the loading pulse to be smoothed. Fig. 6(a) shows the flow at an angle of attack, and Fig. 6(b) shows the flow at zero angle of attack. In Fig. 6(c) the stream lines from Fig. 6(a) have been rotated clockwise by an angle equal to twice the angle of attack, and overlaid onto the zero angle of attack case. The trajectories of the vortices are now almost identical. For the angle of attack case the vortices on the upper (suction) side of the airfoil pass closer to the leading edge singularity than the vortices on the lower (pressure) side of the airfoil. For a blade vortex interaction, as considered in the previous section, the proximity of the vortex to the leading edge singularity is the dominant feature that affects the magnitude and shape of the unsteady loading pulse. When the blade is at a positive angle of attack a vortex passing above the blade will always cause a larger unsteady loading pulse than a vortex passing below the airfoil. In contrast, for a step gust Fig. 5 indicates that the increased contribution from the vortices on the upper side is offset by the reduced contribution of the vortices on the lower side, and this conclusion is only weakly affected by the airfoil thickness.

3.4. Lift sensitivity diagrams

Fig. 7 shows contours of the unsteady lift as a function of the physical coordinates of the vortex as it convects past the airfoil for three different thickness to chord ratios at an angle of attack of 8°. These pictures reveal the sensitivity of the airfoil to a vortical disturbance as a function of the position of that disturbance in the flow field. For the thickness to chord ratio of 0.15 the sensitivity reaches a maximum at a point displaced about 3% chord ahead of the leading edge on the chord line. Closer to the airfoil surface the sensitivity drops considerably as the airfoil surface is approached. The plots for the thinnest and thickest airfoil show that the location of the maximum lift sensitivity moves away from the surface as the thickness increases. Unsteady drag sensitivity values can be plotted in the same way [19] and are typically one quarter of those of the unsteady lift. The trailing edge does have a noticeable influence, locally distorting both the lift and drag contours (not shown).

The same results are shown in Fig. 8 in terms of the initial vortex position Ψ/Ua and time Ut/a which are identical to the non-dimensional drift coordinates of the flow (where Ψ is the mean flow stream function). These pictures show quite explicitly the effect of flow distortion on the response. In physical coordinates the point of greatest sensitivity appears ahead of the airfoil leading edge, on the suction side of the stagnation streamline. The same maximum appears at positive values of Ψ in drift coordinates. Asymmetry is also introduced because of the way the distortion affects the relative timing of events on the upper and lower surfaces. Since the travel time of fluid passing to the suction side of the airfoil is significantly shorter than that of fluid passing to the pressure side, events occurring at the same physical position are dislocated in time across the streamline $\Psi = 0$. A good example is the response features associated with the trailing edge, that are significantly advanced on the suction side and retarded on the pressure side and thus are not phase aligned.

Fig. 9 shows the same the lift sensitivity as a function of location in the circle plane for the different airfoil thicknesses. These also show how the peak lift sensitivity moves away from the surface as the thickness is increased.

Further insight into the sensitivity close to the leading edge is obtained by considering the leading edge pulse in more detail. Using Eq. (15) in Eq. (13) and retaining only those terms which are singular at $z_0 = -a+2\lambda$ gives

$$(F_x + \mathrm{i}F_y)_v \approx \frac{-\mathrm{i}\rho\gamma_o}{2}\left\{\frac{a_c V(Z_o)}{z_c + a_c} + \left(\left(\frac{az_c}{a_c z_o}\right)^2\left(\frac{a_c V(Z_o)}{z_c + a_c}\right)\right)^*\right\} + \cdots, \tag{25}$$

where $z_c = z_0 - \lambda$ and $a_c = a - \lambda$. The unsteady lift from the leading edge pulse is then obtained by multiplying Eq. (25) by $-\mathrm{i}\exp(-\mathrm{i}\alpha)$ and evaluating the real part so

$$L_{\mathrm{LE}} = -\frac{\rho\gamma_0}{2}\mathrm{Re}\left[\left(1 + \left(\frac{az_c\,\mathrm{e}^{\mathrm{i}\alpha}}{a_c z_0}\right)^2\right)\left(\frac{a_c V(Z_0)\mathrm{e}^{-\mathrm{i}\alpha}}{z_c + a_c}\right)\right]. \tag{26}$$

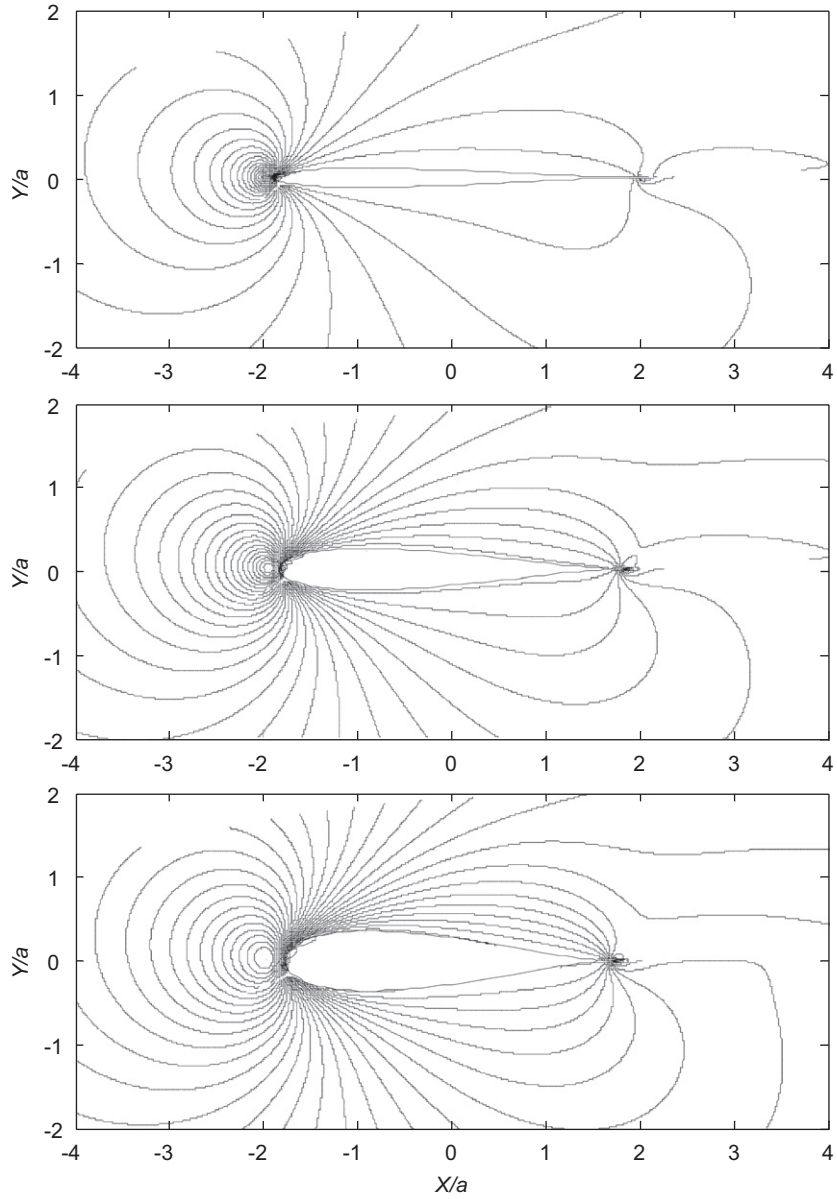

Fig. 7. Unsteady lift sensitivity plots for airfoils of thickness to chord ratios of 0.06, 0.15 and 0.24 for an angle of attack of 8°. Contours show the magnitude of the unsteady lift for each vortex location in the physical plane (X/a, Y/a).

The velocity is given by

$$V(Z_0) = \left(\frac{(1 - a/z_0)(1 + a\,\mathrm{e}^{2\mathrm{i}\alpha}/z_0) U\,\mathrm{e}^{-\mathrm{i}\alpha}}{1 - (a_c/z_c)^2} \right)^*. \tag{27}$$

In the leading edge region the function L_{LE} is quite complicated with a second-order pole at $z_c = -a_c$ and a zero at the stagnation point $z_0 = -a\exp(-2\mathrm{i}\alpha)$. The influence of the singularity will dominate the lift sensitivity close to the leading edge, and so we can assume that when $z_0 \sim -a$ we can approximate $az_c = a_c z_0$, so

$$L_{\mathrm{LE}} \approx -\frac{\rho \gamma_0 U_\infty}{2} \mathrm{Re}\left[\left(1 + \mathrm{e}^{2\mathrm{i}\alpha}\right) \left(\frac{a_c^3 (z_0 + a\,\mathrm{e}^{2\mathrm{i}\alpha})^*}{a^2 |z_c + a_c|^2} \right) \right]. \tag{28}$$

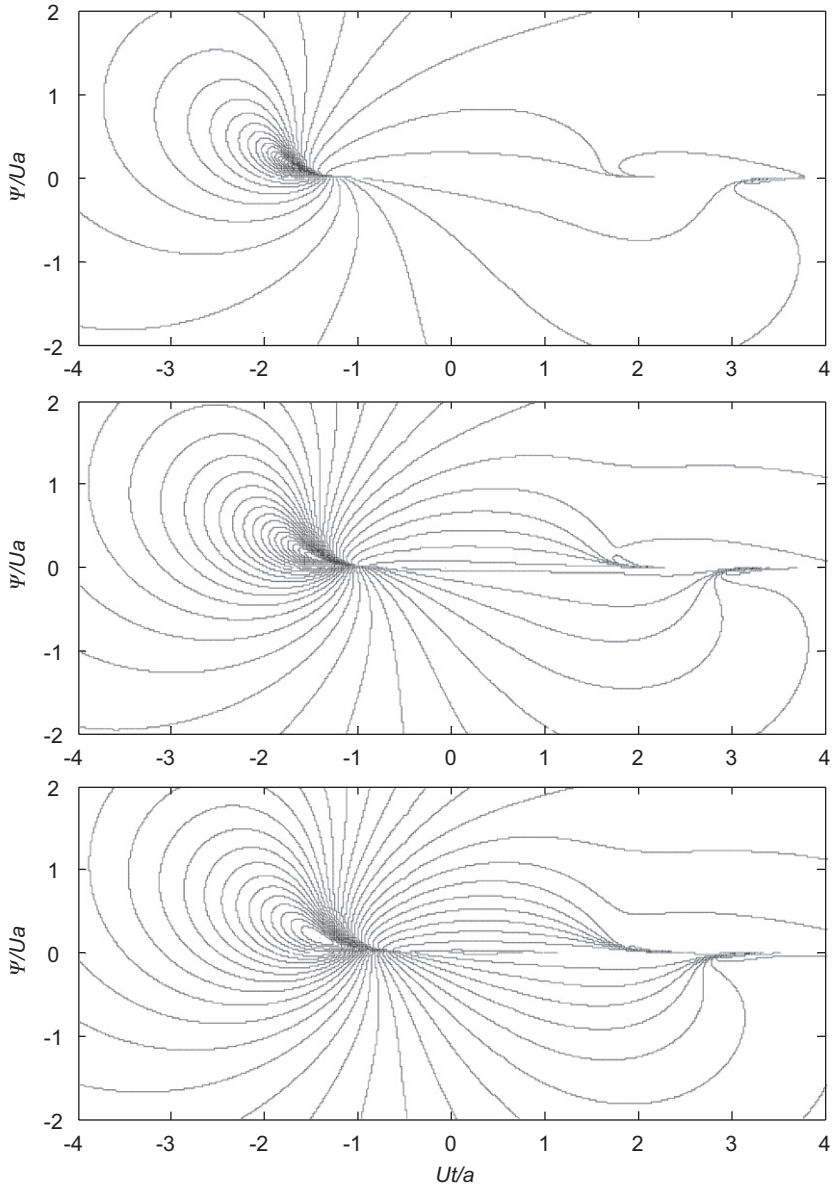

Fig. 8. Unsteady lift sensitivity plots for airfoils of thickness to chord ratios of 0.06, 0.15 and 0.24. Contours show the magnitude of the unsteady lift for each vortex location in drift coordinates (Ut/a, Ψ/Ua).

The largest values of this function occur when the vortex lies on the real axis and if this function is evaluated for $z_0 = x_0$ we find

$$L_{\mathrm{LE}} \approx -\frac{\rho\gamma_0 U_\infty}{2}\left(\frac{a_c^3(x_0+a)(1+\cos(2\alpha))}{a^2(x_0+a-2\lambda)^2}\right). \tag{29}$$

The function has a zero at $x_0 = -a$ and by differentiating with respect to x_0 we find it also has a maximum at $x_0 = -a-2\lambda$, which is upstream of the leading edge and dominates the contour plots in Figs. 7–9.

The interesting feature about the lift sensitivity plots is that they show the unsteady lift peaks as the vortex passes the leading edge, but if the vortex is too close to the leading edge the response is reduced. The maximum

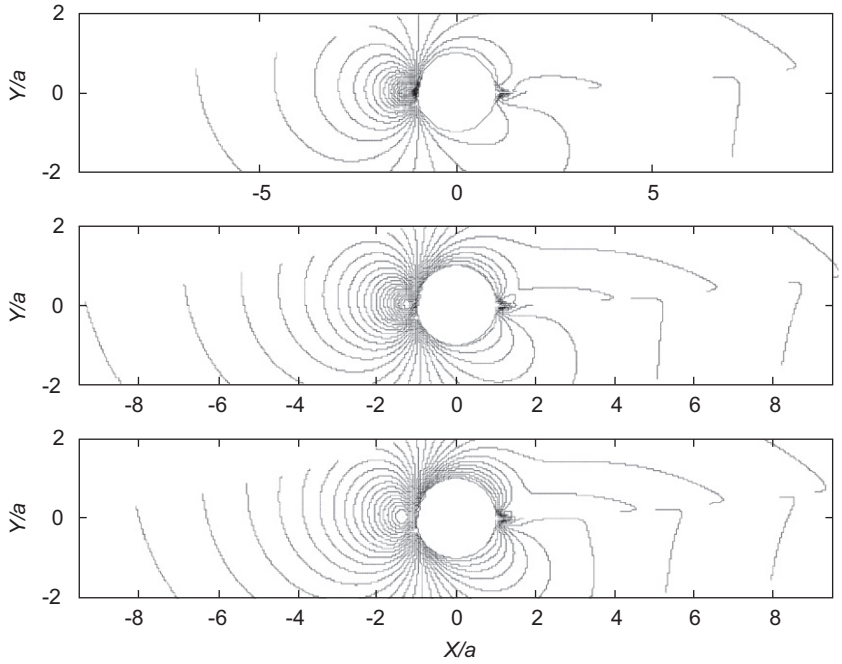

Fig. 9. Unsteady lift sensitivity plots for airfoils of thickness to chord ratios of 0.06, 0.15 and 0.24. Contours show the magnitude of the unsteady lift for each vortex location in the circle plane (x/a, y/a).

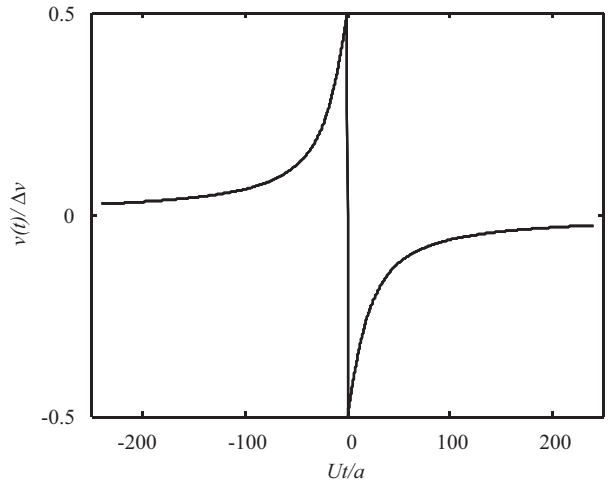

Fig. 10. The upwash gust velocity for a vortex sheet of unit strength, which is used in the calculations of lift spectra. The upwash $v(t)/\Delta v$ is plotted as a function of non-dimensional time Ut/a (Note airfoil chord is $\sim 4a$).

level occurs when the vortex passes at a distance 2λ in front of the leading edge in the circle plane. The location of this maximum moves upstream and its magnitude is reduced as the thickness is increased.

3.5. Unsteady lift spectra

The spectral characteristics of the unsteady lift will be illustrated by taking the Fourier transform of the unsteady loading time history for the step function gust used in Section 3.3. The gust is generated by an array

of equally spaced point vortices along a line which is initiated at 90° to the stagnation streamline at a point which is 30 chord lengths upstream of the center of the airfoil. The vortices are separated by $4a/100$ and the minimum displacement from the stagnation streamline is $4a/200$ (it is shown in Ref. [19] that the spectra converge when the minimum displacement of the vortex is less than $4a/100$). To generate a step function the length of the vortex array should be infinite, but for the purpose of numerical calculations it is limited to $40a$. The resulting upwash gust is plotted as a function of Ut/a in Fig. 10, and is seen to be a rather poor model of a step function, but it does include a step discontinuity at $t = 0$. The spectrum of this gust is shown in Fig. 11 and it is seen to have a slope of $1/\omega^2$ at high frequencies. Some care must be exercised when numerically evaluating spectra for time histories such as those illustrated in Fig. 10. The spectra were calculated with 32,784 points for signatures between $-UT/a < Ut/a < UT/a$ with $UT/a = 240$ and using a window function defined by $\cos^2(\pi t/T)$. The time history was also folded so that the discrete Fourier Transform was applied over $0 < t < 2T$ to a periodic time sequence made up of repeated pulses.

Fig. 12 shows the spectrum of the total unsteady loading $\tilde{F}_T^2(\omega) = |\tilde{F}_L(\omega)|^2 + |\tilde{F}_D(\omega)|^2$ for the airfoil with a thickness to chord ratio of 0.001 at 0°, 4° and 8° angle of attack. Also plotted on this graph is the response obtained by multiplying the gust spectrum by Sears function. Fig. 12 shows that the spectra are independent of

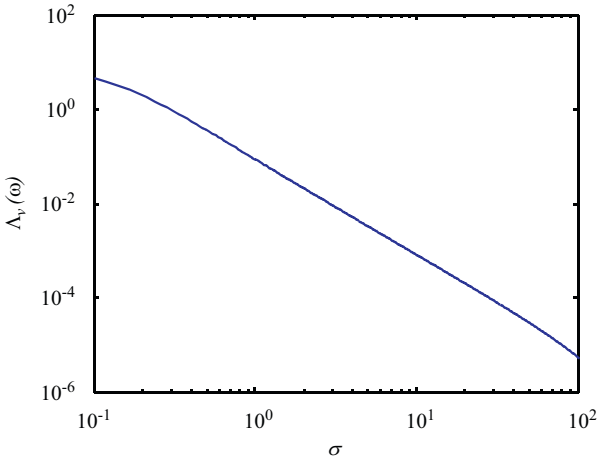

Fig. 11. The spectrum of the gust $\Lambda_v(\omega) = |\tilde{v}(\omega)U/a\Delta v|^2$ used for the calculation of lift spectra as a function of reduced frequency σ.

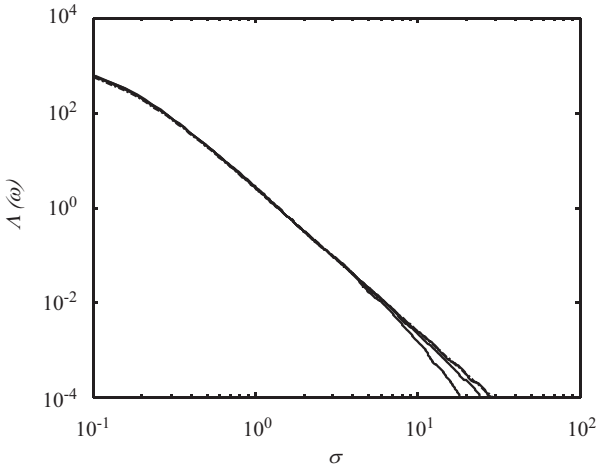

Fig. 12. Unsteady loading spectra $\Lambda(\omega) = |\tilde{F}_T(\omega)/\rho a^2 \Delta v|^2$ as a function of reduced frequency σ for an airfoil with a thickness to chord ratio of 0.001 at angles of attack of 0°, 4° and 8°. (– · –) Spectrum based on Sears function. (—) Spectra for different angles of attack.

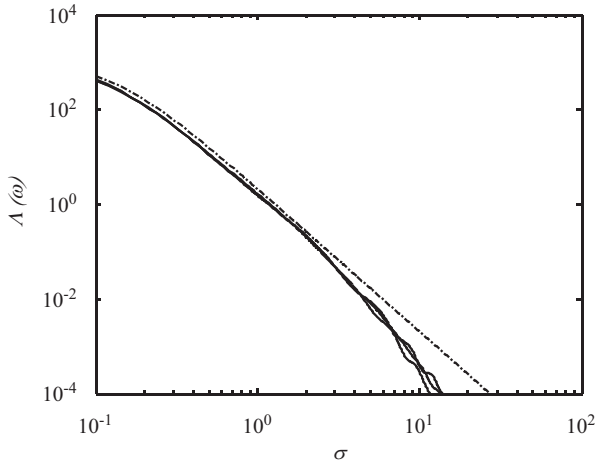

Fig. 13. Unsteady loading spectra $\Lambda(\omega) = |\tilde{F}_T(\omega)/\rho a^2 \Delta v|^2$ as a function of reduced frequency σ for an airfoil with a thickness to chord ratio of 0.15 at angles of attack of 0°, 4° and 8°. (– · –) Spectrum based on Sears function. (—) Spectra for different attack.

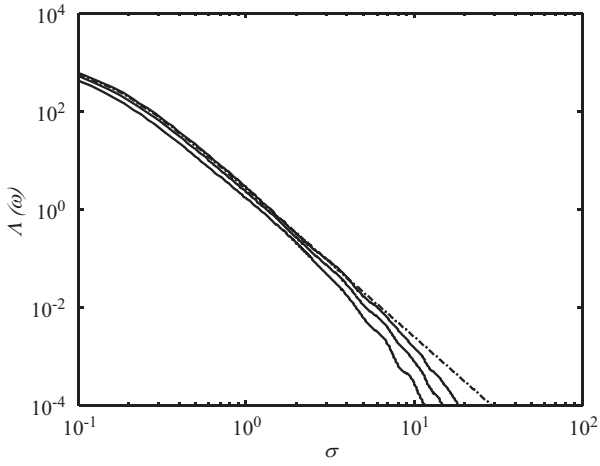

Fig. 14. Unsteady loading spectra $\Lambda(\omega) = |\tilde{F}_T(\omega)/\rho a^2 \Delta v|^2$ as a function of reduced frequency σ for airfoils with thickness to chord ratios of 0.001, 0.06, and 0.15 at an angle of attack of 8°. (– · –) Spectrum based on Sears function. (—) Spectra for different angles of thickness airfoils. Lower levels are thicker airfoils.

angle of attack, confirming our previous conclusions. The only exception is the 8° angle of attack case which deviates from the other results at reduced frequencies above 10, showing a slight decrease in level. Increasing the thickness reduces the rate of change in the gust time history and the high frequency loading response function is reduced as illustrated in Fig. 13, for an airfoil with a thickness to chord ratio of 0.15. Comparing Figs. 12 and 13 shows a reduction in level due to thickness, but the effects of angle of attack remain the same in each case.

Fig. 14 shows the effects of thickness to chord ratio for an airfoil at an angle of attack of 8°. In all cases the amplitude of the response decreases with increased thickness especially at high frequencies. It is interesting to contrast these results with their time histories result with its time history shown in Fig. 15. These show that the signature for the thinnest airfoil has the sharpest change of slope as the gust passes the leading edge, and so we would expect thickness to reduce the spectral level at high frequencies.

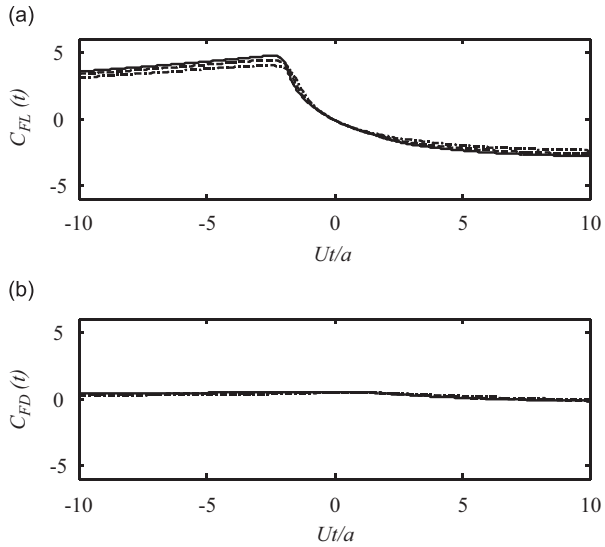

Fig. 15. The unsteady loading coefficients $C_{\mathrm{FL}}(t) = F_L(t)/\rho U\Delta va$ and $C_{\mathrm{FD}}(t) = F_D(t)/\rho U\Delta va$ for a step function incident on an airfoil (see Fig. 5) for airfoils of thickness to chord ratios of 0.001 (solid line), 0.06 (dashed line) and 0.15 (dashed dot line) at 8° angle of attack.

Finally we note that the numerical results presented in this paper based on the analytical approach given in Section 2, have been confirmed using a panel method [19].

4. Conclusions

The unsteady loading on a two-dimensional airfoil in an incompressible flow has been evaluated for an airfoil of arbitrary thickness and angle of attack, without applying the assumptions of thin airfoil theory. It has been shown that the unsteady loading is dominated by the leading edge pulse and the application of the Kutta condition cancels the pulse generated as the gust passes the trailing edge, extending previously known results for flat plates to airfoils of finite thickness and angle of attack.

For a blade vortex interaction the unsteady loading depends on the passage of the vortex relative to the leading edge singularity in the circle plane. As the airfoil thickness is increased this singularity moves to a smaller radius, smoothing the pulse. When the airfoil is at an angle of attack the stagnation point is moved relative to the singularity and the unsteady loading pulse depends on whether the vortex passes the airfoil on the suction or pressure side. If it passes on the pressure side it will always be further from the leading edge singularity than if it passes on the suction side, and so the unsteady loading pulse is reduced.

The characteristics of the unsteady loading are quite different for a step upwash gust, which is more representative of a large scale turbulent flow than a single blade vortex interaction. For a step gust the magnitude of the unsteady loading time history is almost unaltered by changes in angle of attack α but the direction of action of the force is rotated forward so that it makes an angle α with the lift direction. This extends the result obtained by Howe [6] for a flat plate in turbulent flow to an airfoil of arbitrary thickness subjected to a symmetric gust. However spectral analysis of the gust shows that the high frequency blade response is reduced as the thickness of the airfoil is increased.

One of the most important applications of this theory is to airfoils in a turbulent flow. The extension of this analysis to include a turbulent inflow is considered in Ref. [20].

Acknowledgments

This work was supported by the Office of Naval Research, and the authors would like to thank the program manager Dr. Ron Joslin for his encouragement and support.

Appendix A. Numerical evaluation

The unsteady loading is given in Eq. (21) as the sum of the loading from the vortex motion, given by

$$\mathrm{i}\rho\gamma_0\left\{\frac{(a-\lambda)^2}{(z_0-\lambda)^2}\left(\frac{\mathrm{d}z_0}{\mathrm{d}t}\right)+\left(\frac{a^2}{z_0^2}\frac{\mathrm{d}z_0}{\mathrm{d}t}\right)^*+V(Z_0)-U\,\mathrm{e}^{\mathrm{i}\alpha}\right\}, \tag{A.1}$$

and the unsteady loading from the wake given by

$$\mathrm{i}\rho\int_{-\infty}^{t}\mu(\tau)V(X_w)\left(\left\{1+\frac{a^2}{x_w^2}\right\}\frac{(x_w-\lambda)^2}{(x_w-\lambda)^2-(a-\lambda)^2}\right)\mathrm{d}\tau. \tag{A.2}$$

For a vortex in a potential mean flow specified by Eq. (2) it is relatively straight forward to determine the vortex position $z_0(t)$ and velocity $\mathrm{d}z_0/\mathrm{d}t$ and hence evaluate Eq. (A.1) to obtain the time history of the unsteady loading due to vortex motion. For the wake induced load given by Eq. (A.2) the main difficulty is caused by the complexity of the integrand in the convolution integral. To obtain a solution we first assume that the convection velocity of the vorticity in the wake is equal to the mean flow velocity at the trailing edge so $V(X_w)=V_{\mathrm{TE}}=(1-\lambda a)U\cos\alpha$. Then using Eq. (1) we can define the location of the vorticity in the wake as

$$x_w(t,\tau)=\lambda+X_W(t,\tau)/2+\sqrt{(X_W(t,\tau)/2)^2-(a-\lambda)^2}\quad X_W(t,\tau)=2(a-\lambda)+(t-\tau)V_{\mathrm{TE}}, \tag{A.3}$$

The integral in Eq. (A.2) may then be defined as

$$\mathrm{i}\rho\int_{-\infty}^{t}\mu(\tau)q(t-\tau)\mathrm{d}\tau,\quad q(t)=V_{\mathrm{TE}}\left(\left\{1+\frac{a^2}{x_w^2}\right\}\frac{(x_w-\lambda)^2}{(x_w-\lambda)^2-(a-\lambda)^2}\right)_{\tau=0}. \tag{A.4}$$

Using Fourier transforms with the notation convention

$$\tilde{f}(\omega)=\frac{1}{2\pi}\int_{-\infty}^{\infty}f(t)\mathrm{e}^{\mathrm{i}\omega t}\,\mathrm{d}t \tag{A.5}$$

gives Eq. (A.4) as

$$2\pi\mathrm{i}\rho\int_{-\infty}^{\infty}\tilde{\mu}(\omega)\tilde{q}(\omega)\mathrm{e}^{-\mathrm{i}\omega t}\,\mathrm{d}\omega. \tag{A.6}$$

To evaluate the vorticity distribution in the wake we use Eq. (5) with $v_v(t)=\mathrm{i}w_v'(a,t)$ so

$$\tilde{\mu}(\omega)=\frac{a\tilde{v}_v(\omega)}{\tilde{g}(\omega)}\quad g(t)=\left(\frac{x_w+a}{x_w-a}\right)_{\tau=0}. \tag{A.7}$$

We can evaluate Eq. (A.6) numerically by combining it with Eq. (A.7) and using discrete Fourier transforms based on the Fast Fourier Transform algorithm. However some care has to be used in this numerical calculation because both $q(t)$ and $g(t)$ have a singularity of order $t^{-1/2}$ at $t=0$. Accurate numerical approximation of the integrals was achieved by ensuring that the numerical series representing $q(t)$, $g(t)$ and $v_v(t)$ were the same length, used the same time step and satisfied the causality condition. The discrete forms of the time histories were therefore chosen as

$$v_n=v_v(n\Delta t-T),\quad g_n=\begin{cases}0, & n\Delta t<T,\\ g(n\Delta t-T), & n\Delta t>T,\end{cases}\quad q_n=\begin{cases}0, & n\Delta t<T,\\ q(n\Delta t-T), & n\Delta t>T,\end{cases}$$

where $1\leqslant n\leqslant N$ and the time histories are defined at equal intervals Δt. The number of points in the sequence is N and must be a power of 2, so choosing $T=(N+1)\Delta t/2$ ensures that $g(t)$ and $q(t)$ are not evaluated at $t=0$. Numerical evaluation of Eq. (A.6) was then obtained using

$$2\pi\mathrm{i}\rho a\int_{-\infty}^{\infty}\frac{\tilde{v}_v(\omega)\tilde{q}(\omega)}{\tilde{g}(\omega)}\mathrm{e}^{-\mathrm{i}\omega t}\,\mathrm{d}\omega=2\pi\mathrm{i}\rho a\mathrm{DFT}\left[\frac{\mathrm{IDFT}[v_n]\mathrm{IDFT}[q_n s_n]}{\mathrm{IDFT}[g_n s_n]}\right], \tag{A.8}$$

where DFT and IDFT represent discrete forward and inverse Fourier transforms used so that their sign conventions are the same as used in Eq. (A.5). A smoothing function s_n is required to prevent truncation errors at the end points of the integral and $s_n = \cos^2(\pi n\Delta t - T)/2T)$ was found to be effective for this purpose.

Analytical solutions can be obtained for the special case of a flat plate at zero angle of attack. The vortex passes a distance h above the plate and is uniformly convected at the free stream velocity U. The Fourier transform of the wake vorticity is obtained [8] as

$$\tilde{\mu}(\omega) = \frac{2U\tilde{v}_v(a,\omega)e^{i\sigma}}{ia(H_0^{(1)}(\sigma) + iH_1^{(1)}(\sigma))}, \quad \tilde{v}_v(a,\omega) = \frac{a\gamma_0}{2\pi U}(J_0(\sigma) + iJ_1(\sigma))e^{-|\omega h|/U}, \tag{A.9}$$

where $\sigma = 2\omega a/U$ and J_n and $H_n{}^{(1)}$ represent Bessel and Hankel functions of the first kind of order n.

The spectrum of the unsteady lift $L(t) = F_y(t)$ can be obtained from Eq. (24) and is specified using Fourier transforms as

$$\begin{aligned}
\tilde{L}(\omega) &= -\rho U(\gamma_0\tilde{I}^{(+)}(\omega)/2 + 2\pi\tilde{\mu}(\omega)\tilde{q}(\omega)) \\
\tilde{I}^{(\pm)}(\omega) &= \frac{1}{2\pi}\int_{-\infty}^{\infty}\left\{\frac{a}{(z_0 \pm a)} + \frac{a}{(z_0^* \pm a)}\right\}e^{i\omega t}\,dt = \frac{-a\,e^{-|\omega|h/U}}{U}(J_0(\sigma) \mp iJ_1(\sigma)) \\
\tilde{q}(\omega) &= \frac{1}{4\pi}\int_0^{\infty}\left(\frac{x_w - a}{x_w + a}\right)e^{i\omega t}\,dt = \frac{-ia}{4U}\left\{\left[H_0^{(1)}(\sigma) - iH_1^{(1)}(\sigma)\right]e^{-i\sigma}\right\}.
\end{aligned} \tag{A.10}$$

It may be shown that, by introducing Eq. (A.7) and using the Wronskian of the Bessel functions, Eq. (A.8) reduces to the lift spectrum which would have been obtained by using Sears function directly, with the upwash gust specified by the vortex as it is convected past the plate.

References

[1] W.R. Sears, Some aspects of non-stationary airfoil theory and its practical applications, *Journal of the Aeronautical Sciences* 8 (1941) 104–108.

[2] R. Amiet, W.R. Sears, The aerodynamic noise of small-perturbation subsonic flows, *Journal of Fluid Mechanics* 44 (1970) 227–235.

[3] M.E. Goldstein, H.M. Atassi, A complete second order theory for the unsteady flow about an airfoil due to a periodic gust, *Journal of Fluid Mechanics* 74 (1976) 741–765.

[4] H.M. Atassi, The Sears problem for a lifting airfoil revisited new results, *Journal of Fluid Mechanics* 141 (1984) 109–122.

[5] M.S. Howe, On unsteady surface forces, and sound produced by the normal chopping of a rectilinear vortex, *Journal of Fluid Mechanics* 206 (1989) 131–153.

[6] M.S. Howe, Correlation of lift and thickness noise sources in vortex airfoil interactions, *Journal of Sound and Vibration* 137 (1990) 1–7.

[7] M.S. Howe, Unsteady lift and sound produced by an airfoil in a turbulent stream, *Journal of Fluids and Structures* 15 (2001) 207–225.

[8] M.S. Howe, The influence of vortex shedding on the generation of sound by convected turbulence, *Journal of Fluid Mechanics* 76 (1976) 711–740.

[9] M.S. Howe, *Acoustics of Fluid Structure Interactions*, Cambridge University Press, Cambridge, 1998.

[10] J. Gersfeld, Leading edge noise from thick airfoils in turbulent flows, *Journal of the Acoustical Society of America* 116 (2004) 1416–1426.

[11] R. Martinez, J. Rudzinsky, Analytic evaluation of shape effects on blade vortex interactions, Cambridge Acoustical Associates Report U-2466-402.14, 1997.

[12] S.M. Grace, Unsteady blade response: the BVI model vs. the Gust model, *Proceedings of the Seventh AIAA/CEAS Aeroacoustics Conference*, Maastricht, May 2001, AIAA paper no 2001-2209.

[13] D.P. Lockard, P.J. Morris, Radiated noise from airfoils in realistic mean flows, *AIAA Journal* 36 (2001) 907.

[14] D.J. Acheson, *Elementary Fluid Dynamics*, Clarendon Press, Oxford, 1990.

[15] G.K. Batchelor, I. Proudman, The effect or rapid distortion on a fluid in turbulent motion, *Quarterly Journal of Mechanics and Applied Mathematics* 7 (1954) 83–103.

[16] J.C.R. Hunt, A theory of turbulent flow around two-dimensional bluff bodies, *Journal of Fluid Mechanics* 61 (1973) 625–706.

[17] M.E. Goldstein, Unsteady vortical and entropic distortions of potential flows around arbitrary obstacles, *Journal of Fluid Mechanics* 89 (1978) 433–468.

[18] H.M. Atassi, J. Grzedzinski, Unsteady disturbances of streaming motions around bodies, *Journal of Fluid Mechanics* 209 (1989) 385–403.

[19] S. Glegg, W. Devenport, J. Staubs, Leading edge noise, *Proceedings of the 13th AIAA/CEAS Aeroacoustics Conference*, Cambridge, MA, AIAA paper no. 2006-2424-345, May 2006.

[20] S. Glegg, W. Devenport, J. Staubs, Sound radiation from three dimensional airfoils in a turbulent flow, *Proceedings of the 46th AIAA Aerospace Sciences Conference*, Reno, NV, AIAA paper no. 2008-0052, January 2008.